Numerical simulation of a full spine of Edinburgh Duck modules in uni- and multi-directional irregular wave climates, with a view to design optimisation.

Numerical simulation of a full spine of Edinburgh Duck modules in uni- and multi-directional irregular wave climates, with a view to design optimisation.

A. Cotten[1], D. I. M. Forehand

Institute for Energy Systems, School of Engineering, The University of Edinburgh

Abstract

Long, flexibly-jointed spines of Edinburgh Duck modules have the potential to enable the extraction of a large proportion of the wave energy from our seas and oceans. It is well-known that the 'duck' shape is able to efficiently absorb wave energy, and that jointed but controlled interconnections between ducks as part of a full spine can also benefit the performance. However, in order to progress further towards achieving optimal performance in real wave climates, a greater understanding of the significance of the spine configuration and scale, spine orientation, and directional, irregular wave conditions is required. By using an efficient hydrodynamic model of a ten-duck spine in conjunction with a constrained frequency-domain control strategy, this paper investigates the effects of the above factors on device performance (as a function of power extraction) in uni- and multi-directional versions of an irregular wave climate. A series of inferences are drawn from the simulations and discussed with regards to informing the direction of future duck spine designs.

Keywords: Complex conjugate control, Edinburgh duck, generalised modes, hydrodynamic modelling, wave energy converter

1. Introduction

When first proposed as a concept to extract large amounts of energy from sea or ocean waves, long spines comprising many tens of 'duck' modules were envisioned, in order to take advantage of the common reference structure [1]. Since then, many stages of investigation have led to multiple design refinements. With a view to deep-water deployment, the flexibility afforded by rotational roll and yaw joints is necessary between the ducks to avoid significant damage by

Email addresses: alfred.cotten@mocean.energy (A. Cotten[1]), D.Forehand@ed.ac.uk (D. I. M. Forehand)

[1]Corresponding author. Corresponding author's current address: Mocean Energy, Floor 2, Murchison House, 10 Max Born Crescent, Edinburgh, EH9 3BF, UK.

bending moments [2]. Given the subsequent lack of rigidity of the spine, effective designs for a power take-off (PTO) system were required to be housed inside each duck. These were initially provided with the use of a gyroscopic reference frame [3], and more recently by purely hydraulic technology [4][5]. Crucially, these designs retain the absence of a rigid reference point, and enable power conversion that can be continuously controlled. It is also proposed for the hydraulic technology to allow power extraction through the joints, giving full control over most of the degrees of freedom associated with a full spine of ducks. It is this type of integrated, freely-floating system that is required to enable truly significant levels of wave energy extraction from our seas and oceans. Perhaps more importantly, this kind of spine-based system is able to maximally exploit the available sea or ocean space, given the demands of other users. Instead of requiring multiple rows of devices as with conventional wave energy converter arrays, the duck spine aims to extract a much larger proportion of the energy in one go, freeing up space behind.

An efficient numerical model of a long, jointed spine comprising ten duck modules was recently developed by the authors and applied towards investigating the impact of an optimal control strategy on the device performance and dynamics in regular waves [4]. However, the optimal performance of the concept is not only dependent on the control strategy, but also on the shape and scaling of the device, the orientation angle of the spine, and the nature of the surrounding wave climate. By combining the efficient numerical model and optimal control strategy with a spectral and directional representation of a real wave climate, this study aims to establish an understanding of the relationships between the device scale, wave direction (or spine orientation angle), directional spreading and performance (capture width ratio), all with a view towards the optimisation of the spine of ducks.

Similar to the present work, there do exist other studies that have investigated large multi-degree-of-freedom wave energy converter (WEC) systems in a similar manner, with some even including duck-type modules. In one of the earliest applications of the concept of generalised modes (to be explained later) to the modelling of wave energy converters [6], a semi-submersible platform with 21 attached heaving buoys was modelled in the frequency domain. The device performance was even evaluated in a small number of irregular wave conditions, including the effect of wave spreading. However, only a single damping coefficient was applied to each buoy, resulting in a relatively simple control strategy. Additionally, the inertial and gravitational restoring terms were of low complexity, because of the lack of physical coupling between the buoys. The work of [7] also applied generalised modes, in this case to model the ten degrees of freedom of a WEC comprising a floating central cylinder and four surrounding hinged flaps. Again, just a simple damping control strategy was applied to each of the four flaps. In [8], three side-by-side, pitching duck modules were both simulated (using a linear boundary element method approach and using computational fluid dynamics) and experimentally tested, with a view to understanding the interaction effects at different heading angles. A constant damping coefficient was used for all three modules. Finally, the work of [9] again involves pitching

ducks, in that case up to eighteen of them mounted on the three arms of a floating offshore wind turbine platform. Modelling of the system was conducted in the time domain, with each duck controlled by, again, just a damping coefficient. To the authors' knowledge, besides [4], there are no similar studies considering a jointed spine of duck modules, nor considering the application of optimal control to multiple duck modules.

A major contribution of the present paper is the combination of the efficient hydrodynamic model with an optimal (but practically feasible) control strategy and a real wave climate, which enables a system with such a large number of degrees of freedom to be investigated in detail. The paper also brings further implementation details with regards to the use of generalised modes, and incorporates both motion constraints and uncontrolled degrees of freedom into the control theory. Of course, the paper also contributes towards the development and optimisation of a promising yet underexplored WEC concept.

By being able to simulate more than 1.5 million sets of time series, measures of device performance are computed in a (representative) full wave climate for a range of device configurations. The device performance is given in terms of the ratio of power extracted to power present in the waves, on an annual basis. Design recommendations are given in terms of device scaling and orientation, including the impact of directional spreading. The complex device dynamics in a high-energy-extraction sea state are also presented, and used to illustrate the operation of the control strategy on the device motions and power flows. Furthermore, this study shows how monochromatic results can be used to inform the device design in realistic irregular sea conditions.

Herein, the hydrodynamic modelling is conducted in the frequency domain using a boundary element method solver, based on linear potential flow theory. Whilst higher-fidelity approaches (e.g. nonlinear potential flow, computational fluid dynamics, etc. - see e.g. [10]) could allow better incorporation of nonlinear behaviour, the vastly increased runtimes would severely limit the scope of investigation. Though the higher computational demands could be partly alleviated by the used of high-performance computers, this approach typically has the disadvantage of reducing the ability to quickly debug codes and make changes to the setup. Arguably, the only method for efficiently exploring (and potentially optimising) wave energy systems with large numbers of degrees of freedom is the one outlined in this paper, at least with a contemporary personal computer. The semi-analytical method of the complex -conjugate control strategy also maintains low runtime by avoiding the need to model in the time domain. Whilst there are limitations to this approach in terms of the model accuracy, it is worth remembering that for the purposes of improving or optimising designs, accuracy is not paramount as it might be for e.g. performance prediction (see e.g. Section 6.1 of [11]). Regardless, steps to mitigate the inaccuracies of the frequency-domain modelling approach are taken via motion constraints applied to the control strategy and motion limits applied to the time series analysis.

The contents of this article are as follows. Section 2 details the construction of the hydrodynamic model, including specification of the duck and spine design, the underlying modelling assumptions, and some details regarding the

treatment of the large number of degrees of freedom, using generalised modes of motion. The methodology used to derive from the frequency-domain hydrodynamic model an estimation of the power extraction in a multidirectional wave climate is then presented in Section 3. The control strategy is presented in Section 4. The key results regarding the optimal design of a full spine of ducks are presented and discussed in Section 5, followed by the main conclusions in Section 6. Finally, limitations and further work is discussed in Section 7.

2. Hydrodynamic model

Using a single geometry and mass distribution for each duck, the full spine can be modelled efficiently in the frequency-domain using the concept of generalised modes of motion (e.g. [12]). The commercial radiation/diffraction software package WAMIT [13] is used in this study to construct the linear hydrodynamic model, and more information on WAMIT can also be obtained from [14].

Note that the hydrodynamic model used in this study is heavily based upon the model presented in the work of [4], but many details are given again here for completeness. In addition, a more thorough treatment of the implementation of the generalised modes is also presented here.

2.1. Device shape and configuration

Though the duck design used in this study is the same as that used in [4] and [15], for completeness it is worth detailing its geometry and mass distribution here. The design was originally based on the D0018 Medium Beak Duck from [16], which was itself intended as a member of a full spine of ducks. However, some adjustment was necessary to realise a consistent design for the more recent numerical modelling.

In addition to the original six ballast tubes (each of 1.27m diameter), a seventh was added to help achieve the desired mass distribution - see Figure 1. The centre of rotation is located 5m along from the blunt end the 16.8m-long centreline, which itself is angled at 36° to the horizontal in the equilibrium position. Each duck is set to be 29.5m wide (i.e. into the page in Figure 1), with a 10.5m spacing between each pair of adjacent ducks, similar to early models [17], [18].

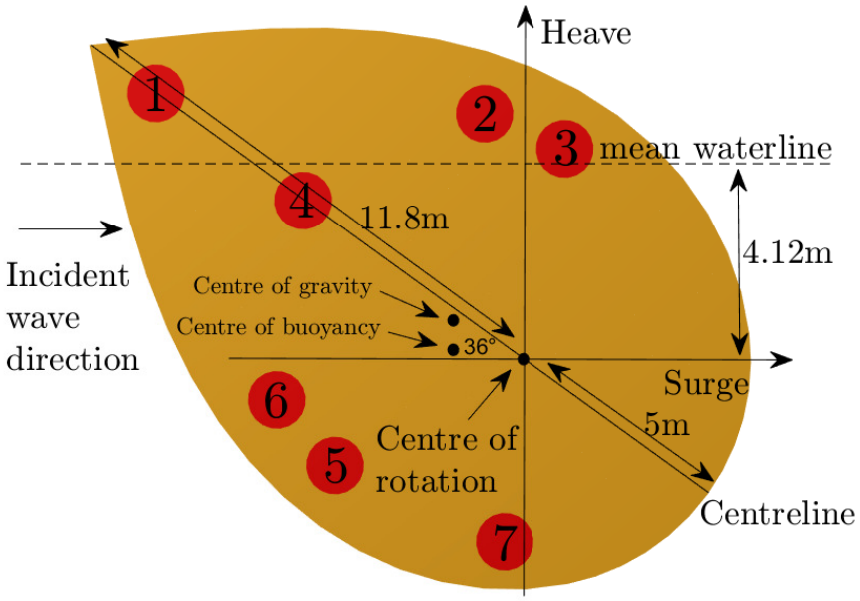

Figure 1: Cross-section of a single member of the full spine of ducks, with the seven ballast tubes displayed. Sway is defined into the page, with the axes centred halfway along the spine length. [Figure reproduced courtesy of [15].]

The mass distribution for each duck must be set to satisfy a number of criteria. Firstly, each duck is set to be statically stable (which in turn, then implies static stability of the whole spine), and to reside in its intended equilibrium position (i.e. the centre of gravity and centre of buoyancy lie on the same vertical line). In addition, the centre of gravity and waterline height must be tuned appropriately. In this design, the chosen ballast masses (specified in Table 1) resulted in a waterline height of 4.12m, and a centre of gravity 1.65m from the centre of rotation, at an angle of 4° anticlockwise from the centreline. This angle is much smaller than the 16° used by Skyner [19] for a solo duck, but is still close to the value of around 10° recommended for good capsize recovery [17].

Ballast index	Mass (tonnes)	Radial position (m)	Angular position (°)
1	0	10	0
2	456	5.5	45
3	312	4.75	65
4	134	6	0
5	0	4.75	-65
6	56	5.5	-45
7	752	4	-120

Table 1: Ballast tube masses and positions for each duck module of the full spine in its original reference configuration. Radial positions are defined from centre of rotation; angular positions are defined clockwise from the part of the centreline joining the centre of rotation and the beak tip (i.e. the pointed edge of the duck).

Because the device scale (in terms of both the cross-section and the width of each of the duck modules) is of interest in this work, it is important to note that the geometry described in this subsection is the original reference configuration - i.e. in the terminology of Section 5, it is the device with scale multiplier = 1.

The full spine investigated herein consists of ten ducks, which is deemed the minimum number to achieve adequate stability by spanning multiple wave crests [2]. To visualise the device, first consider a rigid spine with 5 degrees of freedom (or 'modes' of motion) - surge, sway, heave, roll and yaw, but not pitch. Adding to this spine 10 ducks, each of which can undergo pitch rotation, and 9 interconnecting joints, each of which enables rotation in the roll and yaw directions, results in a 33 degree of freedom system (5 + 10 + (9 x 2)). Figure 2 shows the front, plan and side views of the ten-duck spine, along with the numbering conventions for the ducks (black numbers) and joints (red numbers), and the definitions of the axes and wave direction. More clearly, a heading of 0° corresponds to a predominant wave direction perpendicular to the long axis of the spine, and a heading of 90° corresponds to a wave direction along the spine.

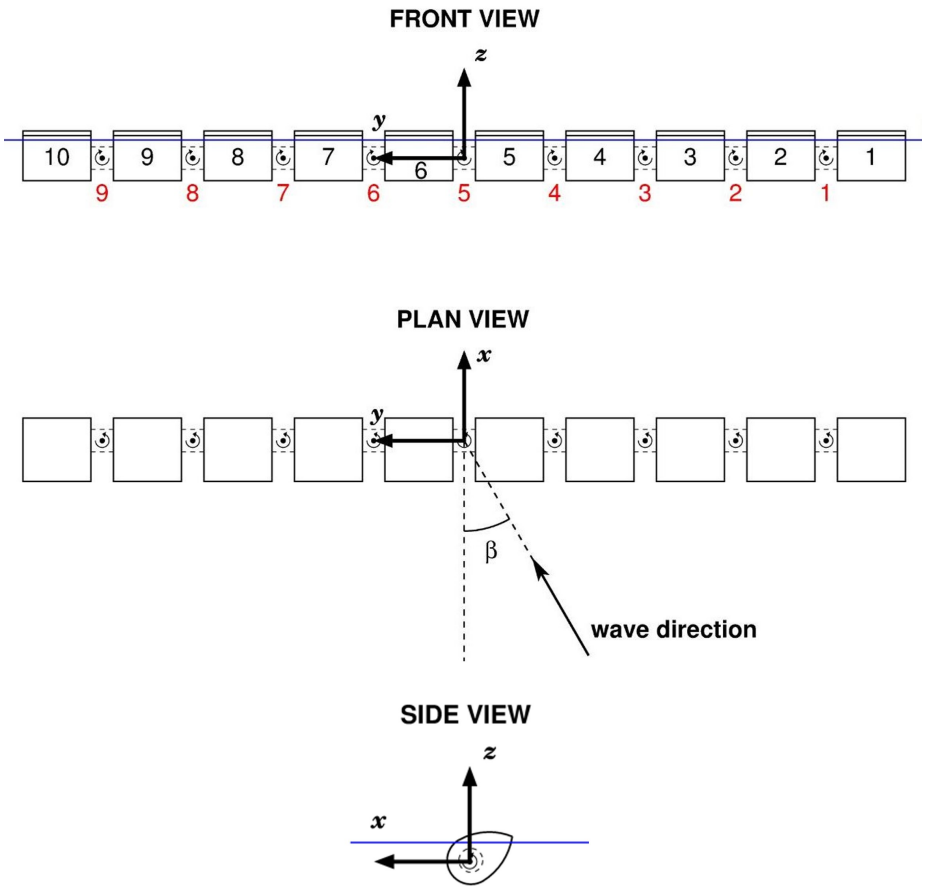

Figure 2: Front, plan and side views of the ten-duck spine, including its two-degree-of-freedom joints. The axis convention and the numbering convention for the ducks and joints are indicated.

2.2. Modelling assumptions

In practice it may be beneficial to allow additional surge motions between each pair of adjacent ducks in order to maintain the correct separation even under bending of the spine, but this is not relevant under the small displacements assumed in the linear numerical model. The internally-housed power take-off systems also remove the need for any additional degrees of freedom, under the assumption that the desired torques could always be provided by the internal mechanisms. In this way, the effect of each power take-off system can be simulated by the application of damping and stiffness torques to the pitch degree of freedom of the corresponding duck module. It is important to note that this

study is not concerned with the state of development of this type of power take-off technology; instead, an idealised PTO system is used for the modelling. The hydrodynamic and inertial properties of the connections between the ducks are neglected, and so the discretised mesh (see Fig. 3, which only displays two of the ten duck modules) for the whole spine only needs to take into account the shape of the ducks and the spacings between them.

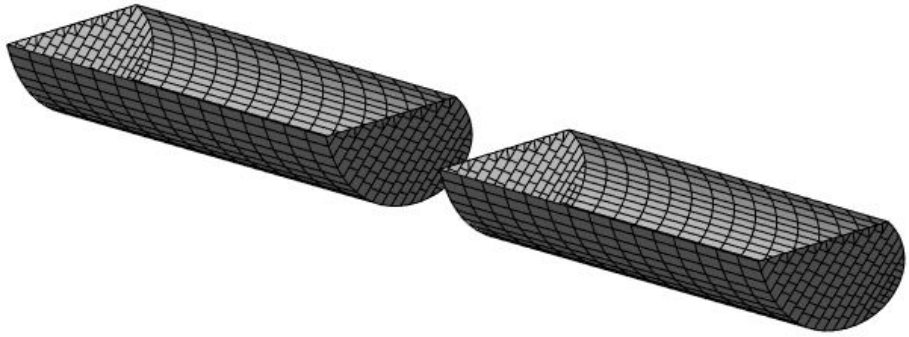

Figure 3: A subsection of the discretised mesh used to compute the hydrodynamic forces that act on the submerged part of the ten duck spine. [Figure reproduced courtesy of [4].]

2.3. Defining the device motions

By specifying additional types of motion over and above the six standard, 'rigid body' degrees of freedom (surge, sway, heave, roll, pitch and yaw), generalised modes enable the formulation of the frequency-domain device dynamics entirely within the linear boundary value problem. This results in an efficient hydrodynamic model of the device, which does not require any post-processing in order to impose the hinge constraints.

Appropriate shape functions [12] are required in order to define the generalised modes, which, via additional radiation potentials, then enable the computation of the hydrodynamic coefficients and body motions using the same theoretical framework as for rigid body modes. Essentially, the shape functions allow arbitrary types of motion to be described in terms of the spatial coordinates, in just the same way that this is done for surge, sway, heave, roll, pitch and yaw. However, the choice of shape functions is not unique. In the context of the spine of ducks, it is most convenient to define a generalised mode describing a rotation about the centre of rotation for each duck, whilst fixing ('locking') the rigid body pitch mode (which is associated with the entire assembly of ducks). This ensures that pitch motions of each duck are defined relative to a stationary reference frame, so that any damping or stiffness forces are applied as they would be by an internal power take-off. In order for natural provision of the necessary reaction forces either side of each joint, the remaining 18 generalised modes of motion are defined symmetrically about each of the nine joints. This leaves the uncontrolled degrees of freedom of the freely-floating device described by five rigid body modes - surge, sway, heave, roll and yaw of the entire ten-duck

spine, as if it were rigid. Of course, the absolute body motions are described by the summation of the motions of all the degrees of freedom.

All nine joints are in line with the centre of rotation, so the location of each is defined by just its y-coordinate, b_i, as are the modes associated with the pitching of each duck. Reserving the first five modes ($1 \leq i \leq 5$) for the rigid body motions (of the entire device), the shape functions for the pitching of each duck are given by Eq. 1:

$$\mathbf{S}_i(\mathbf{x}) = \begin{bmatrix} z \\ 0 \\ -x \end{bmatrix} \text{ for } y \in V_i \text{ and } 6 \leq i \leq 15, \tag{1}$$

where V_i denotes the volume associated with the duck with pitch mode, i. Note, modes 6-15 here correspond with ducks 1-10 in Fig. 2.

The symmetrical shape functions for the joint rotations about the x-axis (akin to roll) are given by Eq. 2, whilst those for the joint rotations about the z-axis (akin to yaw) are given by Eq. 3. These discontinuous generalised modes are defined over the entire body (i.e. all ten ducks). Again, note that the nine roll and nine yaw modes correspond to joints 1-9 as labelled in Fig. 2.

$$\mathbf{S}_i(\mathbf{x}) = \begin{bmatrix} 0 \\ \mp z \\ \pm(y - b_i) \end{bmatrix} \text{ for } y \lesseqgtr b_i \text{ and } i \in I_r := [16, 18, 20, 22, 24, 26, 28, 30, 32] \tag{2}$$

$$\mathbf{S}_i(\mathbf{x}) = \begin{bmatrix} \mp(y - b_i) \\ \pm x \\ 0 \end{bmatrix} \text{ for } y \lesseqgtr b_i \text{ and } i \in I_y := [17, 19, 21, 23, 25, 27, 29, 31, 33] \tag{3}$$

For example, consider shape function $\mathbf{S}_{18}(\mathbf{x})$ - this corresponds to roll motion about the second joint along the spine. For all upstream mesh panels (that is, the mesh elements describing ducks 1 and 2 - see Fig. 2), positive motion corresponds to positive roll (as defined by a shape function, $[0, -z, (y - b_i)]^T$), and for all downstream panels (that is, ducks 3 - 10), positive motion corresponds to negative roll (as defined by a shape function, $[0, z, -(y - b_i)]^T$). Overall, this gives a mode defined by symmetric motion about joint 2.

2.4. Further implementation details

Whilst the shape functions are a necessary starting point in constructing the efficient hydrodynamic model, there are a number of subsequent steps involved. The shape functions enable the computation of the hydrodynamic coefficients, excitation forces and the hydrostatic (or buoyancy) forces for all 33 degrees of freedom. However, in order to compute the device dynamics, the inertial and gravitational restoring forces and moments are also required. These are defined as volume integrals involving the shape functions, and in this case have been

computed numerically in MATLAB. More information on this process was given in Appendix B of [11] and so it is not covered any further here.

WAMIT software was used to solve for the hydrodynamics and hydrostatics. The generalised modes were implemented with the "newmodes" approach (see Section 9.3 of [13]), whereby the shape functions for the 28 generalised modes were added to the provided Fortran source code as a custom subroutine. An Intel Fortran compiler was then used to compile the source code into a dynamic link library file, prior to running the WAMIT executable.

3. Power calculation

In order to compute the power extraction from irregular waves in a given sea state, the frequency-domain body responses from the hydrodynamic model can be superimposed with weightings based on the governing wave spectra. This section presents the methodology for computing the mean annual power extraction of the ten-duck spine from a multi-directional wave climate, based on a location around 40km west of the Shetland Islands. Since it is assumed that the directional component of the wave spectrum is independent of the wave frequency, this methodology can be adapted for a uni-directional wave climate by simply removing the directional dependence of the body responses.

Note that the foundation of the methodology set out in this section is the same as that presented in [20], but in this case, with the additional inclusion of wave directionality. Note also that the notation used in this section is presented in Appendix A.

The spectral density function, $S(\omega_k, \theta_l)$, assigned to the West Shetland Shelf wave climate [21] is based on a modified Pierson-Moskowitz wave spectrum (p. 24, [22]) and a directional spectrum (p.35, [23]) with $n = 4$, defined for $|\theta_l - \beta| \leq 90°$:

$$S(\omega_k, \theta_l) = S(\omega_k)D(\theta_l), \tag{4}$$

where

$$S(\omega_k) = \frac{0.11}{2\pi} H_{m0}^2 T_z \big(\frac{\omega_k T_z}{2\pi}\big)^{-5} exp\Big[-0.44\big(\frac{\omega_k T_z}{2\pi}\big)^{-4}\Big], \tag{5}$$

and

$$D(\theta_l) = \frac{\Gamma(1+\frac{n}{2})}{\sqrt{\pi}\Gamma(\frac{1}{2}+\frac{n}{2})} cos^n(\theta_l - \beta). \tag{6}$$

The amplitudes of the component waves within the spectrum are then given by

$$\alpha(\omega_k, \theta_l) = \sqrt{2S(\omega_k)D(\theta_l)\Delta\omega\Delta\theta}. \tag{7}$$

The spectrum is represented by 98 frequencies, ω_k, spanning the range of 0.18 to 2.12 rad/s in increments of $\Delta\omega = 0.02$ rad/s, and by 21 angles, θ_l, ranging from -90° to 90° in increments of $\Delta\theta = 10°$.

In order to construct the irregular wave profiles and responses, a random phase, $\psi_{k,l}$, is assigned to each frequency component, ω_k, and to each angular component, θ_l, for each of the 173 sea states. For the purposes of later averaging

out the effects of phase, ten sets of these $98 \times 21 \times 173 = 356034$ random phases are then generated, giving ten wave profiles per sea state. The incident irregular wave profile of a given sea state, for one of the ten sets of random phases, q, is given by the superposition of wave components:

$$\eta_q(t) = \sum_{l=1}^{21} \sum_{k=1}^{98} \alpha(\omega_k, \theta_l) cos(\omega_k t + \psi_{k,l,q}). \tag{8}$$

The response of the body, $x_{j,q}(t)$, in degree of freedom j, with set of random phases q, is related to the incident wave profile by the motion Response Amplitude Operators (RAOs), ξ_j. At each frequency and angle, these are obtained from the equations of motion for the 33 degrees of freedom:

$$\sum_{j=1}^{33} [-\omega_k^2(M_{ij}+A_{ij}) + \mathrm{i}\omega_k(B_{ij}+B_{ij}^{pto}) + C_{ij} + K_{ij}^{pto}]\xi_j = X_i \text{ for } i = 1, ..., 33, k = 1, ..., 98, \text{ and } l = 1, ..., 21. \tag{9}$$

WAMIT is used to compute the frequency-dependent hydrodynamic coefficients - added masses, A_{ij}, radiation dampings, B_{ij}, and wave excitation forces, X_i. To clarify, this includes the hydrodynamic cross-couplings amongst all 33 modes of motion, therefore accounting for the hydrodynamic effects of each duck on all of the other ducks. WAMIT is also used to compute part of the hydrostatic matrix, C_{ij} - the coefficients of the buoyancy forces (for all DoFs), and the gravitational restoring force coefficients for only the rigid body modes (in this case, surge, heave and pitch only). The gravitational restoring terms that involve generalised modes, and the mass matrix, M_{ij}, are computed externally, using the mass distribution of the device (see [11] for more details on this procedure).

The coefficients of the damping and stiffness forces provided by the power take-off systems, B_{ij}^{pto} and K_{ij}^{pto}, are optimised analytically using a constrained form of complex conjugate control (see Section 4), by maximising the monochromatic power absorption at the energy period of each sea state. Since only the 10 duck pitch and 18 joint flexure degrees of freedom are controlled, all elements, B_{ij}^{pto} and K_{ij}^{pto}, that relate to the five rigid body modes are set equal to zero.

Given the wave component amplitudes (Eq. 7) from the spectrum definition (Eqs. 4 - 6), the response of each degree of freedom, j, to each wave component is then given by

$$\chi_j(\omega_k, \theta_l) = \alpha(\omega_k, \theta_l)\xi_j(\omega_k, \theta_l) \text{ for } j = 1, ..., 33, k = 1, ..., 98 \text{ and } l = 1, ..., 21. \tag{10}$$

By superimposing these responses to each wave component using the random phases, the time-dependent body response in a given sea state, $x_{j,q}(t)$, is constructed, for each degree of freedom j, and for each set of random phases q, as

$$x_{j,q}(t) = \sum_{l=1}^{21} \sum_{k=1}^{98} |\chi_j(\omega_k, \theta_l)| cos(\omega_k t + \psi_{k,l,q} + \angle\chi_j(\omega_k, \theta_l)) \text{ for } j = 1, ..., 33 \text{ and } q = 1, ..., 10. \tag{11}$$

Despite the application of motion constraints within the control strategy (see Section 4) for each sea state, motion limits are also applied to each body response time series. (Note the proposed semantic distinction between 'constraints' and 'limits' - here, constraints refer to modification of the control strategy, and limits refer to modification of the resulting time series.) As with the motion constraints, these motion limits, X_j^{lim}, are conservatively set to 0.2rad for joint flexure modes of motion, and 0.5rad for the duck pitch modes of motion.

For each degree of freedom, j, and random phase, q, the power is dependent upon the motions of every degree of freedom via the damping coefficients that couple mode j to each other mode of motion, and is determined by Eq. 12.

$$P_{j,q}(t) = \begin{cases} \sum_{i=1}^{33} \dot{x}_{j,q} B_{ji}^{pto} \dot{x}_{i,q} \text{ for } |x_{j,q}(t)| \leq X_j^{lim} \text{ and } |x_{i,q}(t)| \leq X_i^{lim} \\ 0 \text{ otherwise} \end{cases} \tag{12}$$

(Note that no power is extracted through the five rigid body modes ($1 \leq j \leq 5$), since the corresponding damping coefficients are equal to zero.)

For each time series of the instantaneous power, the mean power (for that sea state, defined by H_{m0} and T_z, degree of freedom j, and set of random phases q) is obtained by integrating over the total duration, $T_{\max}$:

$$\bar{P}(H_{m0}, T_z, j, q) = \frac{1}{T_{\max}} \int_{t=0}^{t=T_{\max}} P_{j,q}(t) dt. \tag{13}$$

In this case, $T_{\max}$ is taken to be the maximum length of any non-repeating time series, equal to $2\pi/\Delta\omega \approx 314$s, for which additional justification is given in [20] . Averaging over the ten sets of random phases and summing the power extracted through each of the 28 controlled degrees of freedom, gives the mean power extracted by the duck spine device in a given sea state:

$$\bar{P}(H_{m0}, T_z) = \sum_{j=6}^{33} \frac{1}{10} \sum_{q=1}^{10} \bar{P}(H_{m0}, T_z, j, q). \tag{14}$$

Lastly, weighting the power in each sea state by its annual occurrence, $\hat{O}$, (see Appendix B) and summing, gives the annual mean power extraction,

$$\bar{P} = \frac{1}{8760} \sum_{H_{m0}} \sum_{T_z} \hat{O}(H_{m0}, T_z) \bar{P}(H_{m0}, T_z), \tag{15}$$

where $365 \times 24 = 8760$ is the number of hours in a year.

In order to allow comparison of differently sized duck spines, a metric termed the "annual mean capture width ratio" (amCWR) is lastly introduced:

$$\text{amCWR} = \frac{\bar{P}}{\bar{J}L}, \tag{16}$$

where L is a characteristic dimension of the device, and $\bar{J}$ is the annual mean wave power available per metre of wave crest and defined by

$$\bar{J} = \frac{1}{8760} \sum_{H_{m0}} \sum_{T_z} \hat{O}(H_{m0}, T_z) J(H_{m0}, T_z) \tag{17}$$

and

$$J(H_{m0}, T_z) = \frac{\rho g^2 H_{m0}^2 T_e}{64\pi}. \tag{18}$$

In this case, the dimension, L, is taken to be the total length of the spine. Whilst amCWR this metric is not necessarily suitable for comparison to other device concepts (see e.g. [4]), it allows a fairer comparison of differently sized spines of ducks.

4. Control strategy

The standard form of complex conjugate control (e.g. [24]) allows the analytical expression of the optimal monochromatic power absorption, in terms of the hydrodynamic coefficients. For purposes of achieving the body motions necessary for optimal power, the required control forces can also be expressed (as damping and stiffness matrices) in terms of the physical properties of the wave absorber (e.g. [25]). However, for wavelengths large relative to the body, the demanded excursions can greatly exceed the bounds of validity of the linear theory. In order to avoid this, the method can instead be applied under a motion constraint, which comprises a contribution from each degree of freedom [26]. By selecting suitable upper bounds for the device motions, the modified theory then results in a control strategy that is likely more achievable in reality, and is optimal under the imposed constraint.

In the presence of uncontrolled degrees of freedom, such as is the case with the spine of ducks, the same method can be used to constrain the controlled (power-absorbing) degrees of freedom [27], after a rewriting of the equations of motion (Eq. 19):

$$\begin{bmatrix} \mathbf{F}_c \\ \mathbf{0} \end{bmatrix} = \begin{bmatrix} \mathbf{Z}_{cc} & \mathbf{Z}_{cf} \\ \mathbf{Z}_{fc} & \mathbf{Z}_{ff} \end{bmatrix} \begin{bmatrix} \mathbf{U}_c \\ \mathbf{U}_f \end{bmatrix} - A \begin{bmatrix} \mathbf{X}_c \\ \mathbf{X}_f \end{bmatrix}, \tag{19}$$

where A is the wave amplitude, subscripts c and f are used to denote components relating to the controlled and uncontrolled modes, respectively, and $\mathbf{Z}$ is the intrinsic impedance defined relative to the velocities, $\mathbf{U}$.

Though complex conjugate control has been both applied in constrained form [26] and applied in the presence of uncontrolled degrees of freedom [27], to the authors' knowledge, the theory of both elements has not been published in combination.

As presented in [27], the equations of motion of the free modes can then be used to rewrite the equations of motion of the controlled modes (Eqs. 20, 21, 22), which allows the application of the same method as given in [26].

$$\mathbf{F}_c = \mathbf{Z}_{cc}^m \mathbf{U}_c - A\mathbf{X}_c^m \tag{20}$$

$$\mathbf{Z}_{cc}^{m} = \mathbf{Z}_{cc} - \mathbf{Z}_{cf}\mathbf{Z}_{ff}^{-1}\mathbf{Z}_{fc} \tag{21}$$

$$\mathbf{X}_{c}^{m} = \mathbf{X}_{c} - \mathbf{Z}_{cf}\mathbf{Z}_{ff}^{-1}\mathbf{X}_{f} \tag{22}$$

Explicitly, this results in the optimal power as given by Eq. 23, where $\mathbf{B}_{cc}$ is the real part of $\mathbf{Z}_{cc}^{m}$:

$$\mathbf{P}(\mathbf{U}_c) = \frac{A^2}{8}\mathbf{X}_{c}^{m\dagger}\mathbf{B}_{cc}^{-1}\mathbf{X}_{c}^{m} - \frac{1}{2}(\mathbf{U}_c - \frac{A}{2}\mathbf{B}_{cc}^{-1}\mathbf{X}_{c}^{m})^{\dagger}\mathbf{B}_{cc}(\mathbf{U}_c - \frac{A}{2}\mathbf{B}_{cc}^{-1}\mathbf{X}_{c}^{m}). \tag{23}$$

The corresponding control matrix, whose real and imaginary parts are the damping and stiffness matrices, $\mathbf{B}^{pto}$ and $\mathbf{K}^{pto}$, is given by Eq. 24, where * denotes the complex conjugate transpose, μ is a constant, and $\mathbf{\Gamma}_c$ is the diagonal matrix of constraint weightings (expressed relative to the velocities):

$$\hat{\mathbf{C}} = \mathbf{Z}_{cc}^{m*} + 2\mu\mathbf{\Gamma}_{c}^{-2}. \tag{24}$$

With application to the spine of ten ducks in this paper, conservative constraint weightings that correspond to displacements of 0.2rad for joint flexure modes and 0.5rad for duck pitching modes are used, as have been previously used in the context of a solo duck [26]. The same weightings have also been used previously in the context of the ten-duck spine [4], where it was suspected that the increased number of degrees of freedom would render these values more conservative.

5. Results and discussion

Before presenting the main results from this study, which focus on the annual mean power production of the entire spine and therefore involve aggregation over a large number of simulated time series (see Section 3), it is worth first illustrating the operation of the numerical model. Whilst it is impossible to delve deeply into each and every one of the time series, an example run condition (Table 2) serves to give a idea of the complexity of the system. The chosen sea state involves relatively high energy production for this device configuration.

Wave type	Unidirectional
Wave heading	20°
Device scale	Original
Zero-crossing period, T_z	9.5s
Significant wave height, H_s	2.75m
Random-phase-set index	4/10

Table 2: Definition of the example run condition used to illustrate the typical level of complexity of the resultant dynamics.

The control torques demanded by the constrained complex-conjugate control strategy and applied to the ducks and intervening joints are shown for the example run condition in Fig. 4. The corresponding motions (Fig. 5) and powers (Fig. 6) are also shown. As one might expect because of the relative magnitudes of the inertial terms in the mass matrix, much larger control torques are applied at the joints than in the duck pitch degrees of freedom. This also has the effect of resulting in larger angular displacements of the ducks in pitch, than of the joints in roll and yaw.

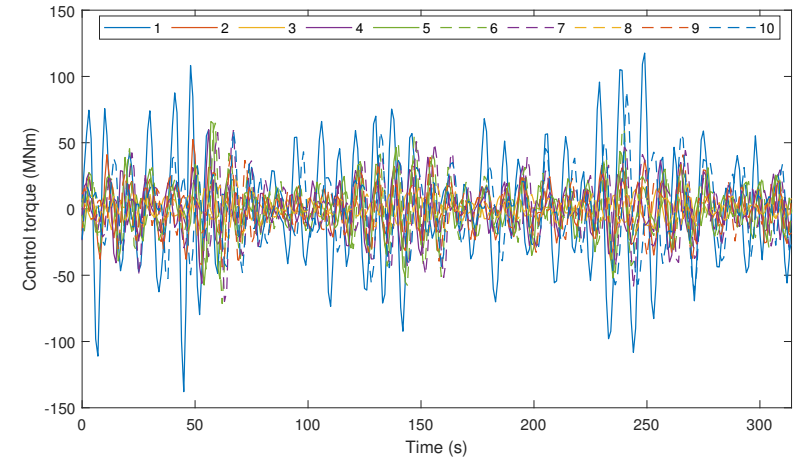

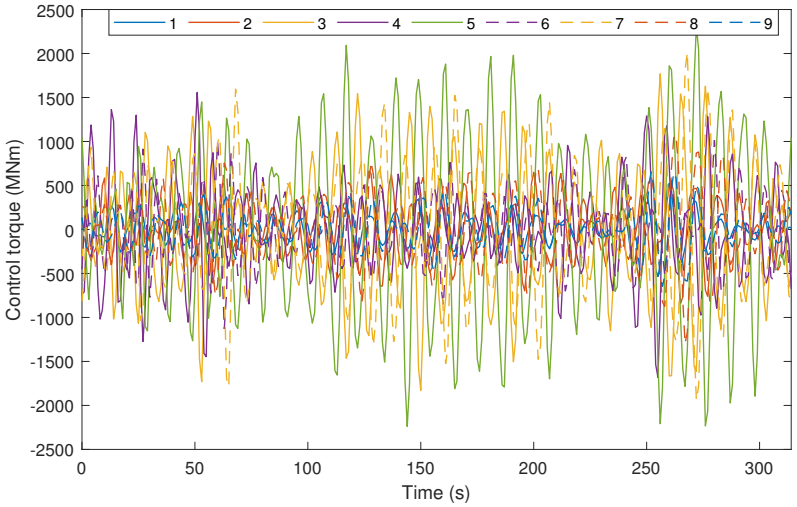

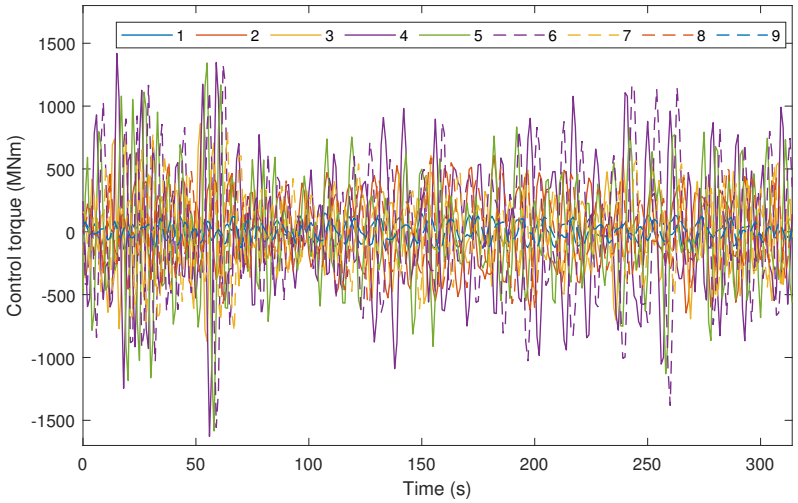

Figure 4: Control torques demanded by the constrained, complex-conjugate control algorithm, as applied to the 28 controlled degrees of freedom (upper plot - duck pitch; middle plot - joint roll; lower plot - joint yaw), in the example run condition. Legend numbering corresponds to the joint and duck numbering convention from Fig. 2.

Within each plot, the significant level of complexity is evidenced by the differing phases and amplitudes of the traces in the numerous degrees of freedom. However, there are a number of key features that stand out. One overarching theme is that the symmetry of the device is reflected (to various degrees) in the time series, yet often this is nuanced by asymmetries likely introduced by shielding and wave diffraction effects. For example, the control torques and motions are often of a similar magnitude for degrees of freedom and their symmetric counterparts (e.g. joint 3 roll and joint 7 roll, or joint 4 yaw and joint 6 yaw) - compare the solid and dashed lines of the same colour in Figs. 4 and 5. However, the phasing is often slightly different (though not always), and can also depend somewhat on the wave crests at a given moment in time.

An interesting case is for roll about joints 3 and 7, where relatively large control torques are applied, often close to in-phase, which yield often in-phase motions and powers. These degrees of freedom also involve the largest amounts of power injection (or reactive power; see Fig. 6), which seems to work in tandem with the roll of joint 5, enabling the large control torques applied there to result in very high power extraction (see the consistent phase relationship between the yellow and green lines in the middle plots in Figs. 4 and 6).

In some cases there are obvious biases in magnitude too - e.g. the control torques applied in pitch to duck 1 (at the front of the spine) are in general larger than those applied in pitch to duck 10 (at the back of the spine).

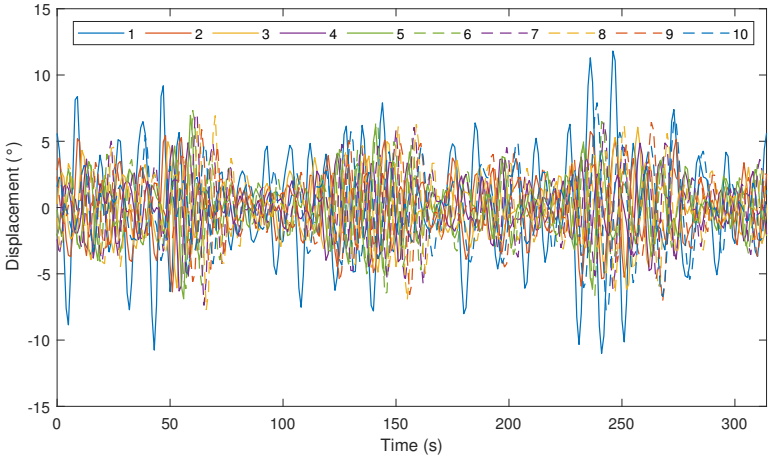
1
2
3
4
5
6
7
8
9
10
Displacement (°)
Time (s)

420

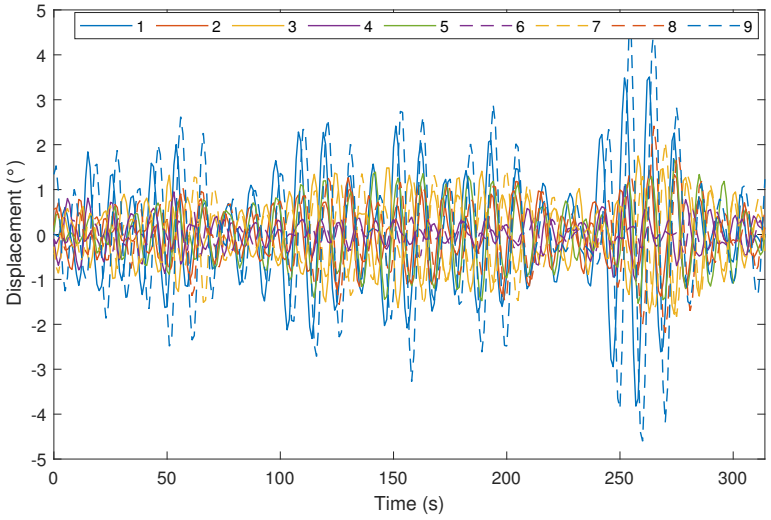
1
2
3
4
5
6
7
8
9
Displacement (°)
Time (s)

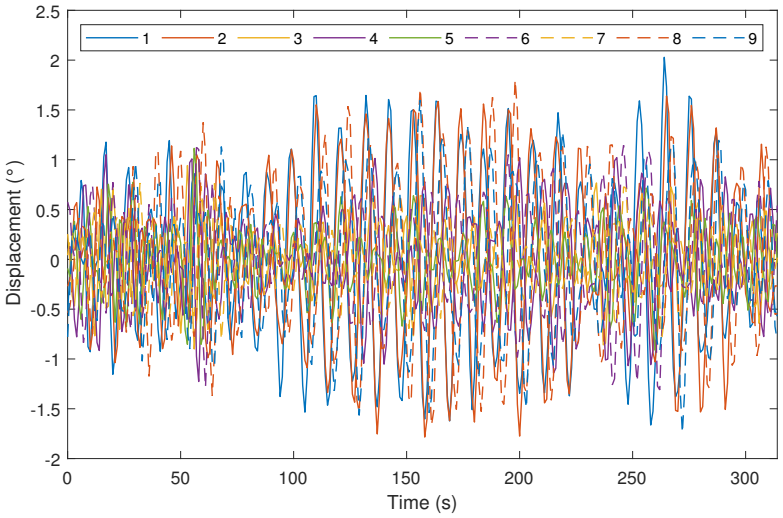

Figure 5: Resultant motions of the 28 controlled degrees of freedom (upper plot - duck pitch; middle plot - joint roll; lower plot - joint yaw), in the example run condition. Legend numbering corresponds to the joint and duck numbering convention from Fig. 2.

It is also evident that little reactive power is supplied through the duck pitching degrees of freedom, and that far more is utilised in the joint flexure modes, in some more than others. The ratio of power extracted to power injected is also dependent on the type of device response, and in turn, the predominant wavelengths at any point in time. For example, relatively larger amounts of reactive power are used during the high-power event around 250s into this example run condition, than elsewhere in the time series.

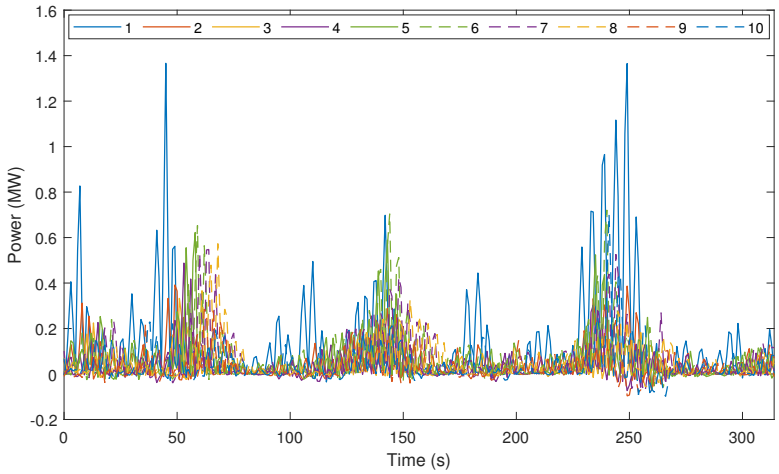

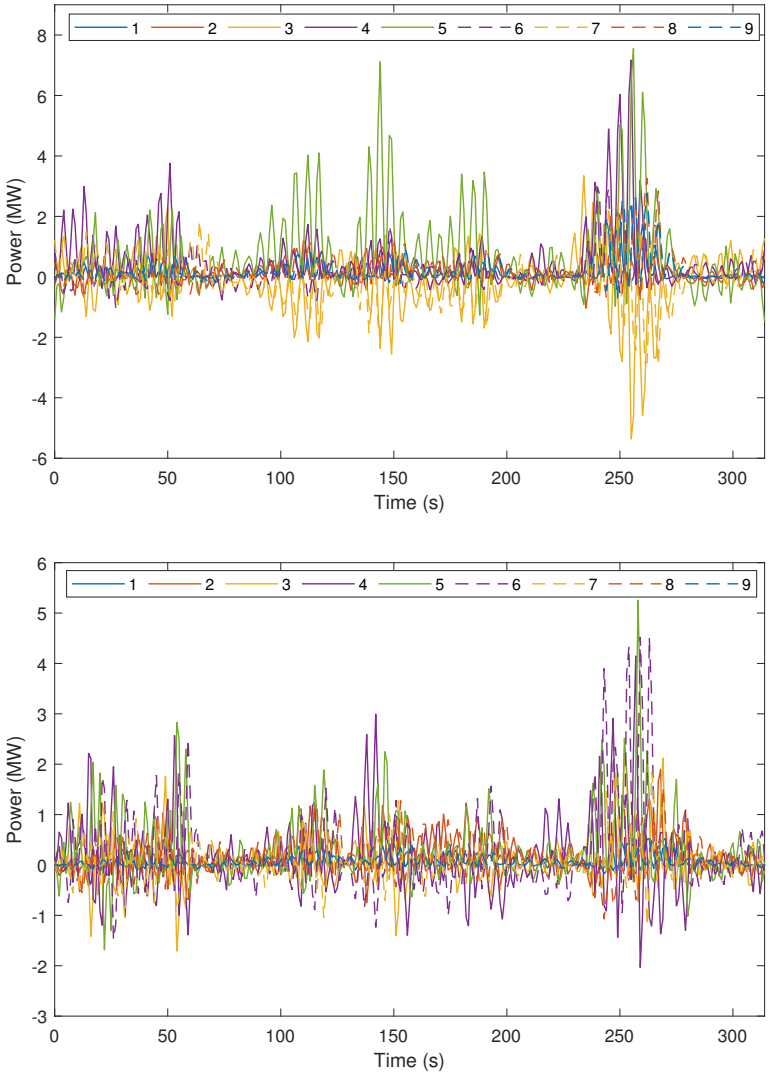

Figure 6: Power extraction (positive) or injection (negative) in each of the 28 controlled degrees of freedom (upper plot - duck pitch; middle plot - joint roll; lower plot - joint yaw), in the example run condition. Legend numbering corresponds to the joint and duck numbering convention from Fig. 2.

Fig. 7 shows the overall power extraction of the device (i.e. the summation of all the curves in Fig. 6). Perhaps interestingly, in this case, though there is power injection in various degrees of freedom at various instants in time, overall, the device is always in net power extraction.

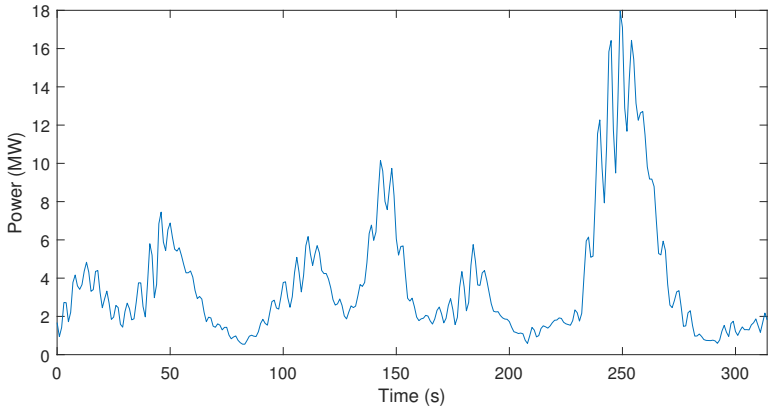

Figure 7: Overall power extraction of the device (i.e. the summation over the 28 controlled degrees of freedom) in the example run condition. Legend numbering corresponds to the joint and duck numbering convention from Fig. 2.

Now continuing into the main results of this study, for both uni- and multi-directional versions of the West Shetland Shelf wave climate, the mean annual power extraction has been computed for five (predominant) wave heading angles (0°, 20°, 40°, 60° and 80°) and for two different device scales - the original scale device (as defined in Section 2.1) and a double-scale device (i.e. a device which has each of its geometrical dimensions doubled when compared to the original). In order to further investigate the effect of device sizing or scale, two other versions of the device have been analysed for only the 0° and 20° wave headings - the original spine scaled up by a factor of 1.4, and the original spine whose duck-cross section has been scaled up by a factor of 1.4, whilst the original duck widths and spacings along the spine (and in turn, the spine length) are retained. In total, this comprises 28 cases, each based upon simulation of the 33 degree-of-freedom device in ten instances of the 314s wave trace, and in each of the 173 sea states. For context, this tallies up to 28 x 33 x 10 x 173 = 1598520 sets of time series, of which only 28 were visualised in Figs. 4 - 7). Values of the annual mean Capture Width Ratio (amCWR) are then computed according to Eqs. 16 - 18 (Figs. 8, 9). For the original-scale and double-scale devices, plots of Capture Width Ratio (CWR) have also been generated for monochromatic waves, of periods between 4 and 24s (in increments of 0.1s) and angles between 0 and 90° (in increments of 10°), with the same constrained version of the complex conjugate control algorithm applied at each period-angle pair (Figs. 10, 11).

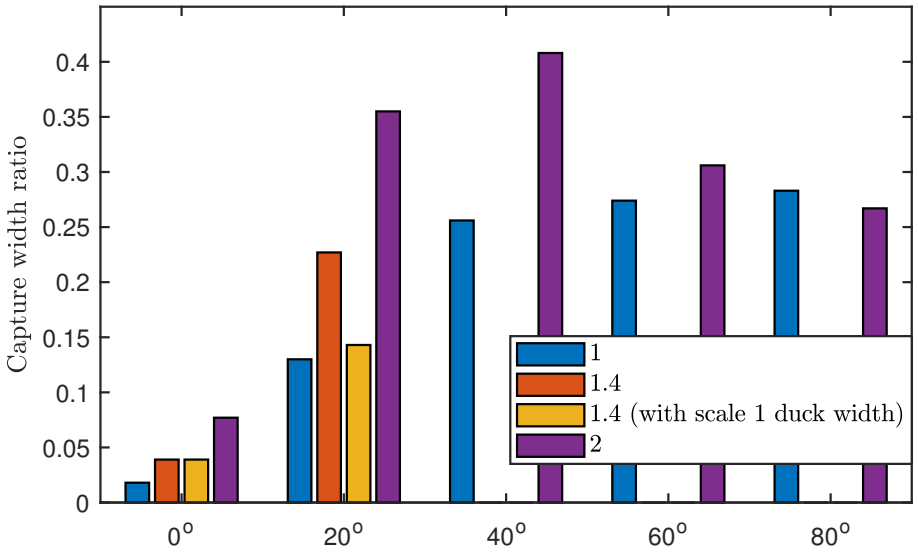

Figure 8: Annual mean capture width ratio (amCWR) of the differently-sized duck spines in the uni-directional, irregular wave climate, for various wave heading angles (labelled on the horizontal axis). Legend indicates the device scale relative to the original design as set out in Section 2.1.

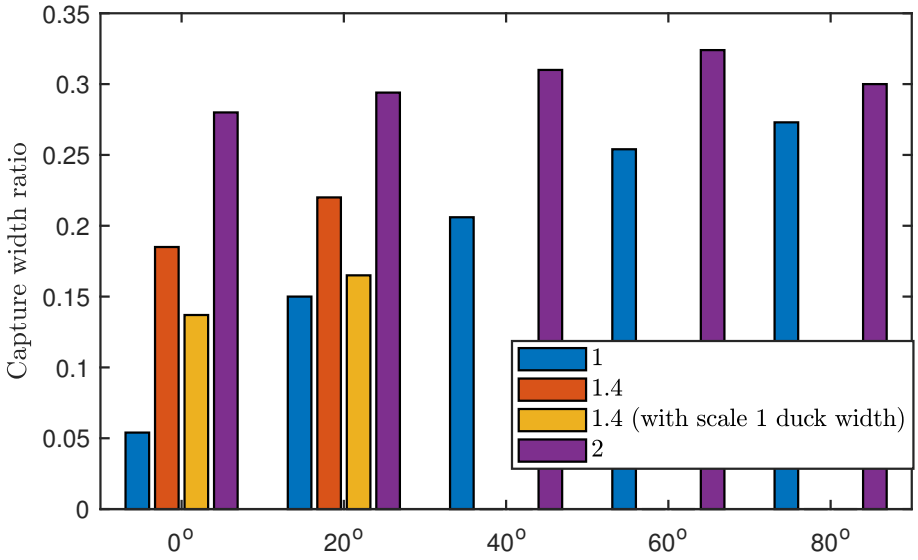

Figure 9: Annual mean capture width ratio (amCWR) of the differently-sized duck spines in the multi-directional, irregular wave climate, for various wave heading angles (labelled on the horizontal axis). Legend indicates the device scale relative to the original design as set out in Section 2.1.

The scale of the device is critical in determining its performance. For lower wave heading angles, the original-scale device is geometrically tuned for optimal performance at wave periods much lower than the most prevalent and energy-intensive periods of the wave climate (compare Fig. 10 with Table B.3 in Appendix B, which is the sea state occurrence matrix.). Therefore, at least for wave angles not exceeding 60°, increases in the scale of the device are accompanied by increases in annual mean capture width ratio - and this effect is more pronounced towards the smallest wave angles (see Figs. 8, 9). At wave heading angles between 60 and 90°, the original-scale device attains peak CWR at a monochromatic wave period of around 16s (Fig. 10), which corresponds closely with the irregular wave conditions in which a large proportion of the energy is contained. For this reason, increases in wave angle always result in increases in amCWR for the original-scale device, despite the peak (monochromatic) CWR value falling as the wave angle increases beyond 30°. For the double-scale device, the band of peak CWR (Fig. 11) intersects a wave period of around 16s at a 40° wave heading, which matches the angle at which the peak value of the uni-directional amCWR occurs.

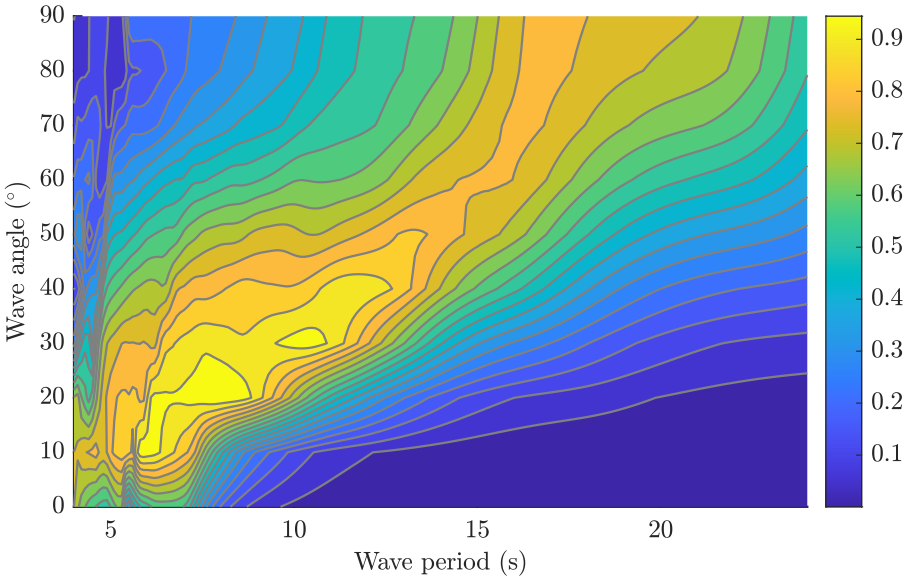

Figure 10: Capture width ratio of the original-scale ('x1') duck spine in monochromatic waves.

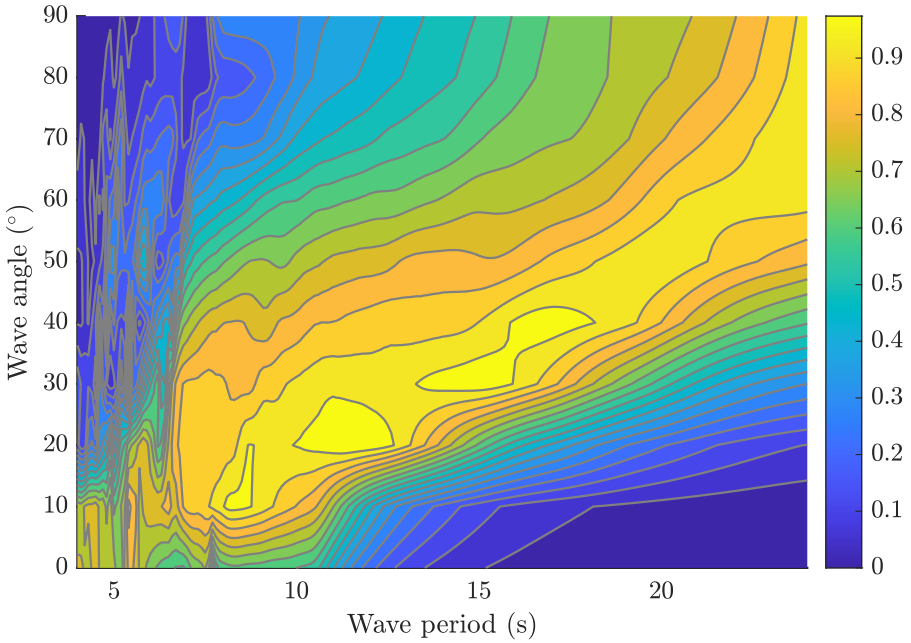

Figure 11: Capture width ratio of the double-scale ('x2') duck spine in monochromatic waves.

At the lowest wave angles where there is minimal engagement of the spine joints between ducks, the performance is most dependent on the scaling of the cross-sections of the ducks. This is further evidenced by the indifference of the amCWR to a change of spine length, under head-on waves - see the leftmost red and yellow bars of Fig. 8. Conversely, at the highest wave angles where the wave propagation direction is nearly parallel to the spine, the performance is most dependent on the axial spine properties (in this study, represented by the scaling along the direction of the spine axis). The moments of inertia are much larger in the roll and yaw joint degrees of freedom than the duck pitch degrees of freedom. Whereas a relatively high CWR of approximately 0.6 is attainable in head-on waves, it is only sustained over a relatively narrow band of small wave periods (Fig. 10), and the duck cross-sections of even the double-scale device are not big enough to exploit this, with a steep decline in CWR beyond 10s (Fig. 11). This is also reflected by the amCWR in head-on unidirectional waves (Fig. 8), and suggests that the duck cross-section should be enlarged further, so as to increase the threshold for the steep decline in CWR from 10s to at least 16s.

However, it should be noted that a sloped band of peak CWR (such as in Figs. 10 and 11) would allow the device to be tuned to different sea states by adjusting the spine orientation angle. If the duck cross-section were enlarged such that the band of peak CWR became near to vertical, annual performance measures may actually be degraded (i.e. because the device would no longer be able to tune to a range of wave periods). In any case, even a small amount of

directional spreading may be sufficient to eliminate the necessity of a potentially less stable duck of much larger cross-section. This can be seen by contrasting the purple bars of both Fig. 8 and Fig. 9. These show that as a function of the (predominant) wave angle, the amCWR is much more narrow-banded in unidirectional seas. In multidirectional seas, the double-scale duck spine sees much less variation in amCWR across the full range of predominant wave angles (see the purple bars of Fig. 9) - a feature which could be beneficially exploited (using the device sizing) in wave climates of varying predominant wave direction. Of course, the peak value of amCWR (with respect to predominant wave angle) would be lower in a wave climate with more spreading, but with the benefit of mitigating either the need for larger duck cross-sections, or for greater demands placed on a system controlling the spine orientation angle in order to avoid head-on waves. Nevertheless, amongst the smaller amount of variation in the amCWR values, the optimal angle of orientation of the spine (60°) is greater than for the case with no directional spreading (40°). This is likely because of the steeper decrease in CWR below the band of peak CWR than above it (Fig. 11). In other words, the (symmetric) directional spreading results in the device effectively sampling a range of the monochromatic CWR values either side of the predominant wave direction, so the asymmetry in CWR with respect to wave direction then results in a bias towards larger predominant wave headings..

It may be difficult or even entirely infeasible to usefully adjust the orientation angle of a full spine of ducks whilst in operation, if the spine end points cannot be moved by large amounts. Alternatively, in order to achieve the optimal amCWR in wave climates with little directional spreading, but with a changing predominant wave direction, it may be possible to employ a zigzag spine arrangement, so that the orientation angle of each duck is then achieved by actuation at the joints, with the axis of the entire spine remaining unchanged. Whilst each duck could face the same wave angle, the orientation of each duck would be opposite to that of its immediate neighbours, so further work is required to verify whether or not this configuration could retain the high performance of the spine design investigated in this paper.

6. Conclusions

Enabled by the development of an efficient model based upon generalised modes of motion, a jointed spine comprising ten Edinburgh ducks and 33 degrees of freedom has been simulated within a range of both uni-directional and multi-directional irregular wave climates, in conjunction with a constrained frequency-domain control strategy. By computing the annual mean Capture Width Ratio (amCWR) for a range of wave heading angles and device scales, it has been possible to make a set of inferences with regards to the development of optimal design configurations. It has also become clear that the monochromatic Capture Width Ratio (CWR) plots are usefully indicative of the device performance in the irregular wave climates, so can, and should, also be used to assist the design process.

Given the fixed duck shape considered in this study, the performance (in terms of amCWR) of the device is dependent on the scaling (or sizing) of the device, the orientation of the spine, and the nature of the wave climate, including any directional spreading. The scaling of the device (including the scale of the duck cross-section and the longitudinal spine properties) should be chosen so as to achieve a band of peak monochromatic CWR (in period-angle space) that is sloped to allow tuning to a particular sea state by altering the spine orientation angle, and that extends over the majority of the range of periods encountered within the wave climate. The overall peak CWR should be set to occur at the average energy period of the entire wave climate. As is typical with the original-scale design studied in this work, undersized duck cross-sections are perhaps more likely than too short a spine.

If there exist significant limitations on the mechanism used to tune the spine orientation in each sea state, the presence of directional spreading may be beneficial, by reducing the dependence of the amCWR on the orientation angle. The spreading may also reduce the need for further and potentially destabilising enlargement of the duck cross-sections. If there exists an asymmetry in the rate of decline of the monochromatic CWR above and below the peak CWR band, the directional spreading is also likely to change the required orientation angle with respect to the predominant direction of the incoming waves.

7. Limitations and further work

In order to build on this work, the code could be developed into a full optimisation scheme, with the aim of comprehensively maximising the performance of the duck spine device. This may also include the duck geometry itself, something not considered in this work. There is also an abundance of data generated from the many run cases (over 1.5 million sets of time series), and much insight could be derived from its further analysis. As introduced in the previous section, further work should also look into the possibility of realising a zigzag spine arrangement. Some level of validation should be carried out, with the use of experimental or higher-fidelity model setups. This would also enable checking the appropriateness of the motion constraint weightings of the complex-conjugate control strategy.

Though the duck spine concept has the potential to extract large amounts of wave energy from the seas and oceans, there also are a number of technical challenges associated with its development. Though these are not the subject of this paper, it is worth mentioning a few considerations here. The interconnected nature of the system can potentially lead to flexural waves travelling down the spine (e.g. [18], [4]), which may accentuate motion of and forces acting at the end joints. In particular, larger scale testing will be needed to ascertain the level of structural reinforcement. Though an idealised form of PTO system is considered in this paper, the concept of an on-board gyroscopic or hydraulic PTO will require further testing. Possible arrangements of multiple mooring lines will also need to undergo testing in extreme conditions to ensure their intended operation of slack mooring the device.

Acknowledgement

This work was supported by a studentship provided by the EPSRC through the Wind and Marine Energy Systems Centre for Doctoral Training (award reference 1809924).

Appendix A. Notation

$\mathbf{A}$	added mass matrix
$\mathbf{B}$	radiation damping matrix
$\mathbf{B}^{pto}$	power take-off system damping matrix
$\mathbf{C}$	stiffness matrix
D	directional spectrum
g	gravitational acceleration
H_{m0}	significant wave height
i, j	motion mode indices
q	spectral component phase set index
J	power in irregular waves
$\mathbf{K}^{pto}$	power take-off system stiffness matrix
k	wave frequency index
L	characteristic dimension of device
l	wave angle index
$\mathbf{M}$	mass matrix
n	directional spectrum quantity
P	extracted power
$\hat{\mathbf{O}}$	occurrence matrix
$\mathbf{S}_i(\mathbf{x})$	shape function of mode i
S	spectral density function
T_e	energy period
T_z	mean zero-crossing period
t	time
V_i	volume associated with mode i
X_j^{lim}	motion limit of mode j
$\mathbf{X}$	excitation force vector
$\mathbf{x} = x, y, z$	spatial coordinates
Γ	Gamma function
α	amplitude of component wave
β	predominant wave direction
η	wave elevation
θ	wave angle
ξ	response amplitude operator
ρ	density of water
χ	amplitude of body response to component wave
ψ	random phase
ω	angular wave frequency

Appendix B. The wave climate

The annual occurrence matrix for the West Shetland Shelf wave climate used in this study is given in Table B.3 [21], in terms of mean zero-crossing period, T_z, and significant wave height, H_{m0}. The site is around 40km west of the Shetland Islands.

T_z (s) $\rightarrow$ H_{m0} (m) $\downarrow$	4.5	5.5	6.5	7.5	8.5	9.5	10.5	11.5	12.5	13.5	14.5	15.5	16.5	17.5
0.25	0	2	2	0	0	1	0	0	0	0	0	0	0	0
0.75	36	89	147	128	95	44	18	10	1	4	4	1	0	0
1.25	51	229	228	306	339	215	82	42	12	6	6	1	0	0
1.75	2	115	184	208	302	269	177	92	24	14	4	2	1	1
2.25	0	21	165	184	202	231	205	115	67	26	18	8	1	1
2.75	0	1	63	153	158	142	193	142	84	47	21	11	1	1
3.25	0	0	5	105	147	103	125	136	92	58	30	10	5	1
3.75	0	0	1	31	113	100	89	92	79	48	33	12	3	1
4.25	0	0	0	5	51	86	77	69	53	42	33	14	6	3
4.75	0	0	0	0	20	62	65	51	43	39	31	17	6	2
5.25	0	0	0	0	2	22	59	47	36	28	23	13	2	4
5.75	0	0	0	0	0	5	38	45	23	16	25	10	2	0
6.25	0	0	0	0	0	1	14	39	17	15	21	5	1	1
6.75	0	0	0	0	0	0	4	24	21	13	11	4	2	0
7.25	0	0	0	0	0	0	1	14	17	11	6	2	2	0
7.75	0	0	0	0	0	0	0	8	16	11	4	2	1	0
8.25	0	0	0	0	0	0	0	4	14	10	3	2	1	1
12.00	0	0	0	0	0	0	0	2	19	26	26	11	2	2

Table B.3: West Shetland Shelf occurrence matrix ($\hat{O}$, hours).

For additional reference, the annual energy content (per metre of wave crest) of this climate is displayed in Figure B.12. For each sea state, this has been computed as the product of the wave power per metre wave crest (defined as $\frac{\rho g^2 T_e H_{m0}^2}{64\pi}$) and the corresponding entry in the occurrence matrix of Table B.3.

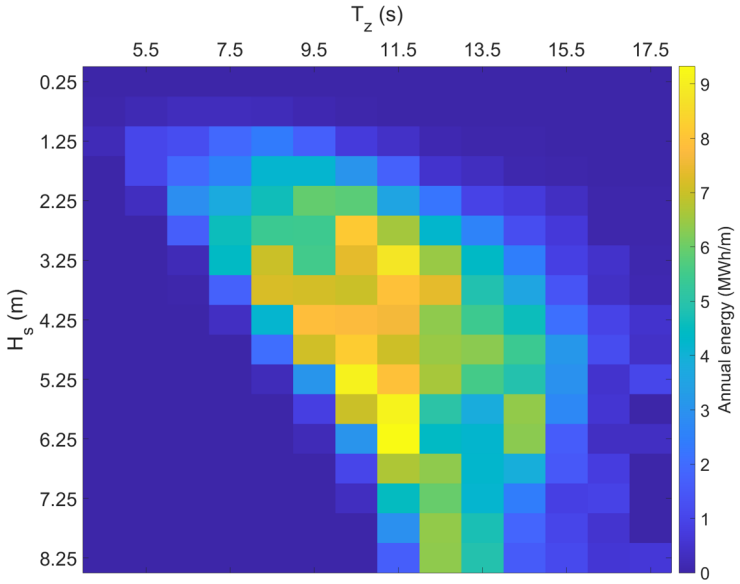

Figure B.12: West Shetland Shelf annual energy (per metre of wave crest) matrix.

Note the omission of the bottom row of the occurrence matrix from inclusion in Figure B.12. Though there are relatively high amounts of energy in a small number of these sea states, the overall amount of energy contained in these is only a small fraction of the total annual energy. In any case, the application of the motion constraints and motion limits prevents the WEC systems from harnessing much of this energy.

References

[1] S. H. Salter, Wave power, Nature 249 (1974) 720–724, DOI: 10.1038/249720a0.

[2] S. Salter, Wave energy: Nostalgic ramblings, future hopes and heretical suggestions, Journal of Ocean Engineering and Marine Energy 2 (2016) 399–428, DOI: 10.1007/s40722-016-0057-3.

[3] S. H. Salter, The use of gyros as a reference frame in wave energy converters, Proceedings of the 2nd International Symposium on Wave Energy Utilization, Trondheim (1982) 99–115.

[4] A. Cotten, D. I. M. Forehand, Investigation into the control strategy for a long spine of Edinburgh Duck modules, using an efficient numerical model, International Marine Energy Journal 3(3) (2020) 145–154. doi:10.36688/imej.3.145-154.

[5] S. Salter, private communication, 2019.

[6] R. Taghipour, T. Moan, Efficient frequency-domain analysis of dynamic response for the multi-body wave energy converter in multi-directional waves, Proceedings of the Eighteenth International Offshore and Polar Engineering Conference (2008) 357–365.

[7] G. Sismani, E. Loukogeorgaki, Frequency-based investigation of a floating wave energy converter system with multiple flaps, Applied Mathematical Modelling 84 (2020) 522–535. doi:10.1016/j.apm.2020.04.013.

[8] S. K. Poguluri, D. Kim, Y. H. Bae, Hydrodynamic analysis of a multibody wave energy converter in regular waves, Processes 9 (2021) 1233. doi:10.3390/pr9071233.

[9] H. Yazdi, H. R. Ghafari, H. Ghassemi, G. He, M. Karimirad, Wave power extraction by multi-salter's duck wecs arrayed on the floating offshore wind turbine platform, Energy 278 (2023) 127930. doi:10.1016/j.energy.2023.127930.

[10] Folley, M. (Ed), Numerical Modelling of Wave Energy Converters: State-of-the-art techniques for single devices and arrays, Elsevier, London, UK, 2016.

[11] A. Cotten, D. I. M. Forehand, Optimisation of a novel, sloped module, multibody wave energy converter, using an efficient modelling technique, Renewable Energy 162 (2020) 727–742. doi:10.1016/j.renene.2020.07.091.

[12] J. N. Newman, Wave effects on deformable bodies, Applied Ocean Research 16 (1994) 47–59. doi:10.1016/0141-1187(94)90013-2.

[13] WAMIT User Manual (v7.4), WAMIT Inc., http://www.wamit.com/manual.htm, Accessed: 09/01/2023.

[14] C.-H. Lee, J. N. Newman, Computation of wave effects using the panel method, WIT Transactions on State-of-the-art in Science and Engineering 18 (2005) 211–251. doi:10.2495/978-1-85312-837-0/06.

[15] A. Cotten, D. Forehand, Maximum wave-power absorption under motion constraints associated with both controlled and uncontrolled degrees of freedom, Applied Ocean Research 100 (2020) 102194. doi:https://doi.org/10.1016/j.apor.2020.102194.
URL https://www.sciencedirect.com/science/article/pii/S0141118719310557

[16] D. C. Jeffrey, D. J. E. Richmond, S. H. Salter, J. R. M. Taylor, Second year interim report on Edinburgh wave power project: "Study of Mechanisms for Extracting Power from Sea Waves", Edinburgh Research Archive (1976, accessed on 09/01/2023).
URL http://hdl.handle.net/1842/23410

[17] D. C. Jeffrey, G. J. Keller, D. Mollison, D. J. E. Richmond, S. H. Salter, J. R. M. Taylor, I. A. Young, Edinburgh Wave Power Project: Fourth Year Report Volume 1 Of 3, Edinburgh Research Archive (1978, accessed on 09/01/2023).
URL https://hdl.handle.net/1842/37385

[18] S. H. Salter, Edinburgh Wave Power Project: "Bending moments in long spines", Edinburgh Research Archive (1984, accessed on 09/01/2023).
URL http://hdl.handle.net/1842/23542

[19] D. Skyner, Edinburgh Wave Power Project: "Solo duck linear analysis", Edinburgh Research Archive (1987, accessed on 09/01/2023).
URL http://hdl.handle.net/1842/23535

[20] A. Cotten, D. Forehand, Multi-objective optimisation of a sloped-motion, multibody wave energy converter concept, Renewable Energy 194 (2022) 307–320. doi:https://doi.org/10.1016/j.renene.2022.05.030.
URL https://www.sciencedirect.com/science/article/pii/S0960148122006681

[21] A. P. McCabe, Constrained optimization of the shape of a wave energy collector by genetic algorithm, Renewable Energy 51 (2013) 274–284. doi:10.1016/j.renene.2012.09.054.

[22] O. M. Faltinsen, Sea loads on ships and offshore structures, Cambridge University Press (1990) .

[23] Environmental conditions and environmental loads, Tech. rep., Det Norske Veritas, available from: https://www.dnvgl.com/oilgas/download/dnvgl-rp-c205-environmental-conditions-and-environmental-loads.html (October 2010).

[24] J. Falnes, Ocean Waves and Oscillating Systems: Linear Interactions Including Wave-Energy Extraction, Cambridge University Press, Cambridge, UK, 2002.

[25] P. Nebel, Maximizing the efficiency of wave-energy plant using complex-conjugate control, Proceedings of the Institution of Mechanical Engineers, Part I: Journal of Systems and Control Engineering 206 (1992) 225–236. doi:10.1243/PIME_PROC_1992_206_338_02.

[26] D. J. Pizer, Maximum wave-power absorption of point absorbers under motion constraints, Applied Ocean Research 15 (1993) 227–234, DOI: 10.1016/0141-1187(93)90011-L.

[27] D. J. Pizer, Edinburgh Wave Power Project: "Numerical modelling of wave energy absorbers", Edinburgh Research Archive (1994, accessed on 09/01/2023).
URL http://hdl.handle.net/1842/23532